small method
www.small-methods.com

Oxidation or Reduction State of Au Stabilized by an MOF: Active Site Identification for the Three-Component Coupling Reaction

*Qihao Yang and Hai-Long Jiang**

As one of the most efficient catalysts for the three-component coupling reaction of aldehyde, amine, and alkyne (A^3 coupling), Au has attracted extensive attention, but there is a debating issue on whether $Au^{\delta+}$ ($\delta > 0$, representing the oxidation state of Au species) or Au^0 is the better active site. According to previous reports, both $Au^{\delta+}$ and Au^0 can catalyze the A^3 coupling reaction. Therefore, the establishment of a suitable comparison model to identify the better active site is highly desired. In this work, an ideal model to identify the efficient active sites for the A^3 coupling reaction based on a metal–organic framework (MOF) platform is rationally fabricated. The $Au^{\delta+}$ in oxidation state can be well bound to the MOF, MIL-101-NH_2, via postsynthetic modification, and the Au^0 catalyst with retained MOF skeleton can be formed via a subsequent one-step reduction, which provide ideal comparison models with the only difference in the Au oxidation state. Strikingly, the two catalysts exhibit significant activity difference in the A^3 coupling reaction. The activity of $Au^{\delta+}$ catalyst is 11-fold higher than that of Au^0, which reveals that $Au^{\delta+}$ serves as a much more effective active site in the A^3 coupling reaction.

Gold, including Au nanoparticles (NPs), salts, complexes, etc., being a class of efficient homogeneous and heterogeneous catalysts, have attracted widespread attention owing to their excellent properties toward a wide range of chemical transformations such as CO oxidation, water gas shift, selective hydrogenation, selective oxidation, C—H bond activation, etc.[1–7] Over the past decades, thousands of gold catalysts have been developed based on a great number of different parameters, including oxidation state, support effect, and coordination environment of Au, etc. These significant differences make it difficult to compare the performance of resultant Au catalysts from different studies, even in the same catalytic reaction. For example, the three-component coupling of aldehyde, amine, and alkyne (also called A^3 coupling) is a representative type of C—H bond activation reaction to produce propargylamine and its derivatives, serving as an important intermediate for the synthesis of many nitrogen-containing biological and pharmaceutical compounds, which can be catalyzed by Au^0 and $Au^{\delta+}$ ($\delta > 0$, representing the oxidation state of Au species) according to the previous reports.[8–12] For example, Liu et al. sythesized an Au/MIL-53(Al) catalyst-containing Au^0 and Au^{3+} species, which display good activity for the A^3 coupling reaction.[13] In addition, Liu et al. also demonstrated the Au^{3+}-containing catalyst, IRMOF-3-LA-Au, can exhibit good performance in the A^3 coupling reaction.[14] Some comparative studies have been attempted, such as the contrastive properties of gold salts and Au^0 sponges, or the activity comparison between Au NPs/PMO (PMO = periodic mesoporous organosilica) and $Au(PPh_3)Cl$.[15,16] Unfortunately, these comparisons have not been able to exactly give the intrinsic property of different Au species due to the presence of different supports, which is a potential factor to affect the activity. There is still an intensive debate on the nature of the gold species involved in the reaction after the elimination of the support effect. Therefore, it is necessary to seek for a suitable model with the only difference in Au oxidation state to identify the efficient active site.

As a relatively new class of crystalline porous materials, metal–organic frameworks (MOFs), featuring high porosity, structural diversity, and tailorability are attracting extensive interest and are employed toward various applications including gas storage and separation, drug delivery, sensing, catalysis, etc.[17–25] MOFs exhibit an unrivalled ability to realize atom-level structural determination and tailoring. Particularly, some particular functional groups with strong chelating/anchor ability can be facilely grafted onto the MOF pore walls via either one-step assembly or postsynthetic modification (PSM).[26–28] This character makes MOFs might be ideal supports to stabilize Au^0 and $Au^{\delta+}$ for studying structure–catalytic activity relationship.

With the above considerations in mind, we rationally introduced the salicylaldehyde (SA) and $HAuCl_4$ precursors into a mesoporous MOF, MIL-101-NH_2, via a PSM approach. SA was bound to the MOF via the reaction with the amino group to give corresponding product (denoted as MIL-101-SA) with imine

Q. Yang, Prof. H.-L. Jiang
Hefei National Laboratory for Physical Sciences at the Microscale
CAS Key Laboratory of Soft Matter Chemistry
Collaborative Innovation Center of Suzhou Nano Science and Technology
Department of Chemistry
University of Science and Technology of China
Hefei, Anhui 230026, P. R. China
E-mail: jianglab@ustc.edu.cn

The ORCID identification number(s) for the author(s) of this article can be found under https://doi.org/10.1002/smtd.201800216.

DOI: 10.1002/smtd.201800216

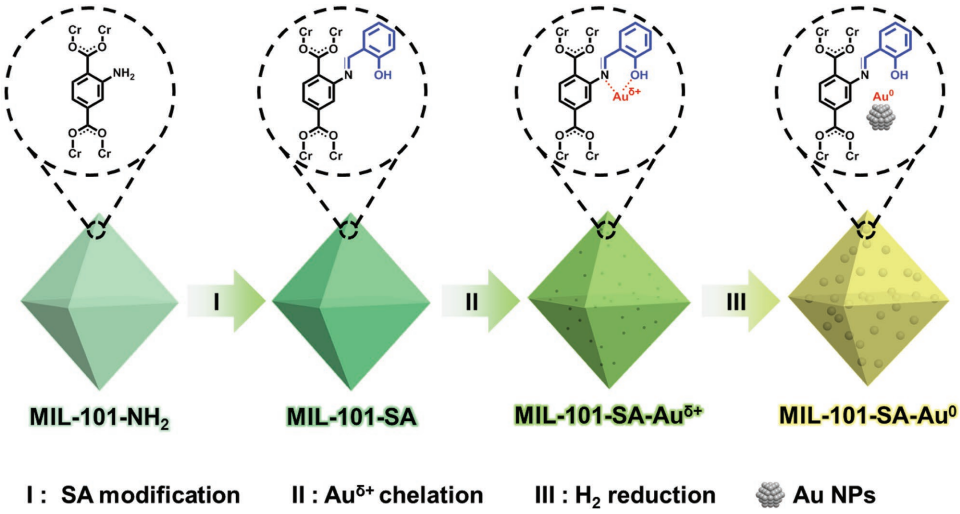

Scheme 1. Schematic illustration of the fabrication process for MIL-101-SA-Au$^{\delta+}$ and MIL-101-SA-Au^{0}.

group. The hydroxyl and imine groups of the resulting MIL-101-SA are able to serve as the anchoring groups to stabilize Au$^{\delta+}$ ions. Subsequently, MIL-101-SA-Au^{0} can be obtained by a reduction process in hydrogen/argon flow (**Scheme 1**). Given that MIL-101-SA-Au^{0} was prepared by the one-step reduction of MIL-101-SA-Au$^{\delta+}$, we believe that the only difference in both catalysts should be the oxidation state of gold. Strikingly, they exhibit significant activity difference in the A^3 coupling reaction: the activity of MIL-101-SA-Au$^{\delta+}$ catalyst is almost 11-fold higher than that of MIL-101-SA-Au^{0}. It is explicitly shown that the oxidative Au$^{\delta+}$ is the more efficient active center than Au^{0}, toward the A^3 coupling reaction.

The mesoporous chromium-based MOF, MIL-101-NH$_2$, was chosen due to its high stability in water, two large cavities, and easily modified amino groups. However, MIL-101-NH$_2$ cannot be obtained by a one-step solvothermal reaction via the coordination binding between Cr^{3+} and 2-aminoterephthalic acid. Alternatively, MIL-101 was initially synthesized via a hydrothermal method,[29] and subsequent nitration by concentrated HNO_3 and H_2SO_4 in an ice-water bath gave MIL-101-NO$_2$. Finally, the nitro groups were reduced to amino groups with the help of $SnCl_2 \cdot 2H_2O$ to yield MIL-101-NH$_2$ (Scheme S1, Supporting Information).[30]

The production of MIL-101-SA was carried out according to the reported procedure with minor modifications.[31] The as-synthesized MIL-101-NH$_2$ was immersed into a CH_2Cl_2 solution containing SA at room temperature for 12 h, which caused a color change from bright green to chartreuse (Figure S1, Supporting Information). This was accompanied with a broadening of the UV–visible absorption spectrum, implying the successful condensation reaction and the imine formation (Figure S2, Supporting Information). Moreover, in reference to MIL-101-NH$_2$, Fourier transform infrared spectrum of MIL-101-SA showed a slightly decreased intensity of the $-NH_2$ vibrations at 3481 and 3377 cm^{-1}, indicating that partial part of amino groups were modified (Figure S3, Supporting Information).[32,33] The ^{1}H NMR spectra were adopted to examine the extracted linker molecules and to determine the modification level (Figure S4, Supporting Information). Results exhibited both signals of 2-aminoterephthalate and imine-terephthalate, indicating that ≈17% of the amino groups were successfully modified in MIL-101-SA. The MIL-101-SA-Au$^{\delta+}$ was synthesized by adding $HAuCl_4$ to the anhydrous CH_2Cl_2 solution containing MIL-101-SA under stirring, and the catalyst was separated after 8 h. Finally, the MIL-101-SA-Au^{0} catalyst was obtained after the reduction treatment in a hydrogen/argon flow at 200 °C. Although, Au/MOF catalysts for A^3 coupling reaction, such as Au/MIL-53(Al), IRMOF-3-LA-Au, etc., have been reported, there are structural differences and advantages of MIL-101-SA-M (M = Au$^{\delta+}$ or Au^{0}) over previous catalysts. Compared with Au/MIL-53(Al) catalyst fabricated via the impregnation method with $HAuCl_4$,[13] the hydroxyl and imine groups of MIL-101-SA can provide strong chelating/anchor sites to immobilize Au ions, rather than being adsorbed on the surfaces or pores of the MOF. Furthermore, in reference to IRMOF-3-LA-Au (LA = lactic acid) catalyst,[14] MIL-101-SA-M exhibits much better water stability that allows the reaction to proceed in water and avoids the use of organic solvent. In a word, MIL-101-SA possesses excellent structural stability and chelating sites to stabilize Au species, making the resulting catalysts steadily catalyze the A^3 reaction in water.

Powder X-ray diffraction (XRD) patterns for MIL-101-SA- Au$^{\delta+}$ and MIL-101-SA-Au^{0} show that the crystallinity and structure of MIL-101-NH$_2$ remain well during the PSM and reduction processes (**Figure 1**a). The absence of diffraction peaks assignable to Au NPs in MIL-101-SA-Au^{0} implies the low Au content and/or the very small Au NPs. The influences of PSM and metal loading on the porosity of MIL-101-NH$_2$ have been evaluated using N_2 sorption at 77 K. It is obvious that the introduction of SA only slightly affects the surface area (from 1894 to 1619 m^2 g^{-1}) of the pristine MOF (MIL-101-NH$_2$). In addition, MIL-101-SA-Au^{0} remains highly porous and its Brunauer–Emmett–Teller (BET) surface area reaches 1103 m^2 g^{-1}. An appreciable decrease in N_2 sorption amount and surface area should be due to the cavity occupation of MIL-101-NH$_2$ by the Au NPs (Figure 1b). The transmission electron microscopy (TEM) images demonstrated that no Au NPs can be observed in MIL-101-SA-Au$^{\delta+}$ but they were well dispersed in MIL-101-SA-Au^{0} with an average size

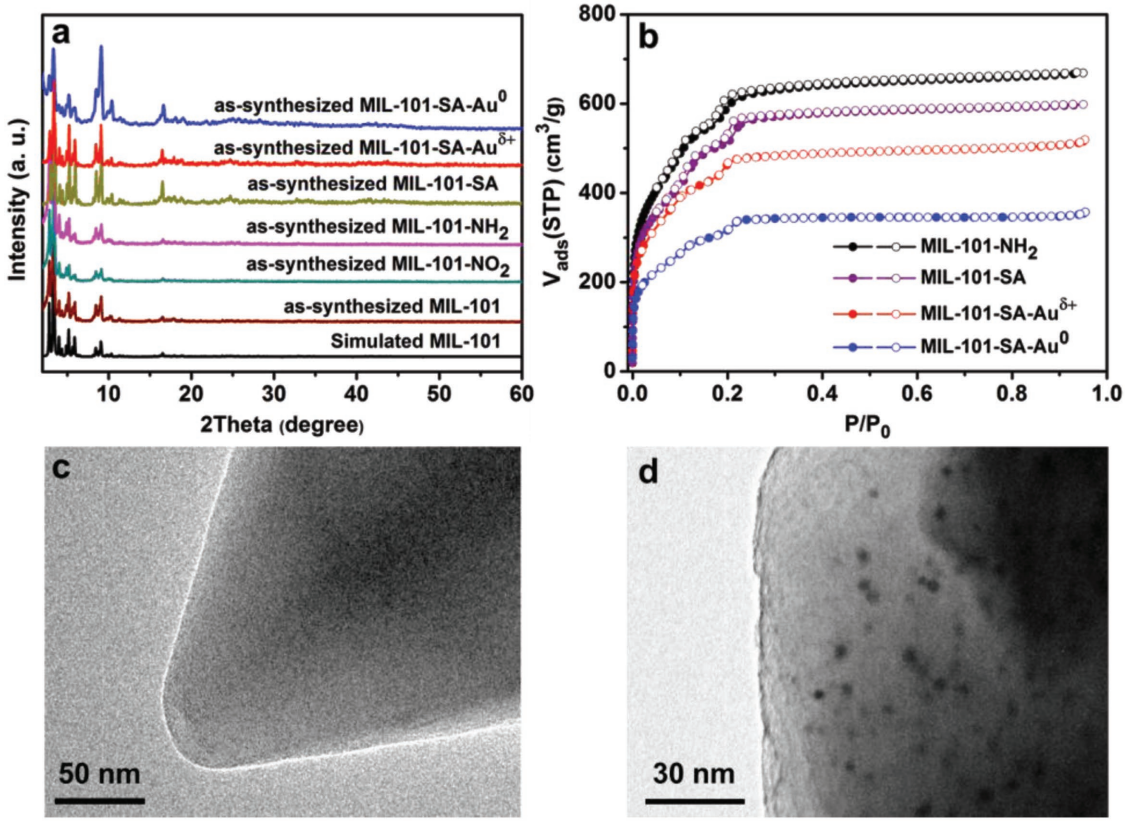

Figure 1. a) Powder XRD patterns of simulated MIL-101, as-synthesized MIL-101, MIL-101-NO_2, MIL-101-NH_2, MIL-101-SA, MIL-101-SA-$Au^{\delta+}$, and MIL-101-SA-Au^0. b) N_2 sorption isotherms for MIL-101-NH_2, MIL-101-SA, MIL-101-SA-$Au^{\delta+}$, and MIL-101-SA-Au^0 at 77 K. TEM images of c) MIL-101-SA-$Au^{\delta+}$ and d) MIL-101-SA-Au^0.

of ≈2.7 nm (Figure 1c,d, Figure S5, Supporting Information), which well matches the cavity size of the MOF, inferring the possible encapsulation of Au NPs in MOF cages. Inductively coupled plasma-atomic emission spectroscopy (ICP-AES) indicated that the actual Au contents for MIL-101-SA-$Au^{\delta+}$ and MIL-101-SA-Au^0 are both ≈0.1 wt%.

X-ray photoelectron spectroscopy (XPS) analysis has been carried out to determine the oxidation state of the Au species in MIL-101-SA-$Au^{\delta+}$ and MIL-101-SA-Au^0. The results present four peaks with binding energies of 84.4, 87.9, 85.1, and 88.9 eV corresponding to Au^0 $4f_{7/2}$, Au^0 $4f_{5/2}$, Au^+ $4f_{7/2}$, and Au^+ $4f_{5/2}$, respectively,[34–37] revealing that both Au^0 and Au^+ species are existed in MIL-101-SA-$Au^{\delta+}$. Moreover, the integral peak area of the XPS spectrum shows that the percentages of Au^0 and Au^+ are 36 and 64, respectively (**Figure 2**a). By contrast, the XPS spectrum for MIL-101-SA-Au^0 shows that the Au 4f region contains two peaks at 84.3 and 88 eV, corresponding to the Au^0 $4f_{7/2}$ and Au^0 $4f_{5/2}$ respectively, which manifests the successful reduction of $Au^{\delta+}$ to Au^0 (Figure 2b).

We are now in a position to investigate the catalytic performance of the two Au catalysts for the A^3 coupling. The reaction is initiated by adding either MIL-101-SA-$Au^{\delta+}$ or MIL-101-SA-Au^0 to the solution in a vial containing aldehyde, amine, and alkyne under magnetic stirring at 80 °C. Paraformaldehyde, phenylacetylene, and piperidine are first employed as a model reaction to compare the activity of MIL-101-SA-$Au^{\delta+}$ and MIL-101-SA-Au^0 (Figure 2c,d). From the perspective of green chemistry, water as an environmentally friendly solvent is adopted to disperse the substrates and catalyst. In the presence of MIL-101-SA-$Au^{\delta+}$, the reaction proceeded in a very high rate and the substrates were almost completely converted to the target product in 1 h. In sharp contrast, the reaction rate of MIL-101-SA-Au^0 was much lower, and it required 24 h to give a comparable yield (94%). The significant difference unambiguously indicates that the $Au^{\delta+}$ site is much more active than the reduced Au^0 toward the A^3 coupling reaction.

To compare the different activities between $Au^{\delta+}$ and Au^0 in a more intuitive way, the turnover frequency (TOF) of both catalysts has been evaluated. Given that only surface Au atoms are able to serve as active sites to participate in the reaction, it is necessary to determine the surface atom ratios, particularly for Au NPs. In the spherical NP approximation, an NP is modeled as a sphere.[38] For a spherical NP composed of a number of atoms (X_{np}), the NP radius (R_{np}), surface area (S_{np}), and volume (V_{np}) are related to the radius (R_a), surface area (S_a), and volume (V_a) of the constituent atoms. The expression is as follows:

$$V_{np} = X_{np}\, V_a \tag{1}$$

By expressing Equation (1) in terms of the NP and atomic radius, we obtain:

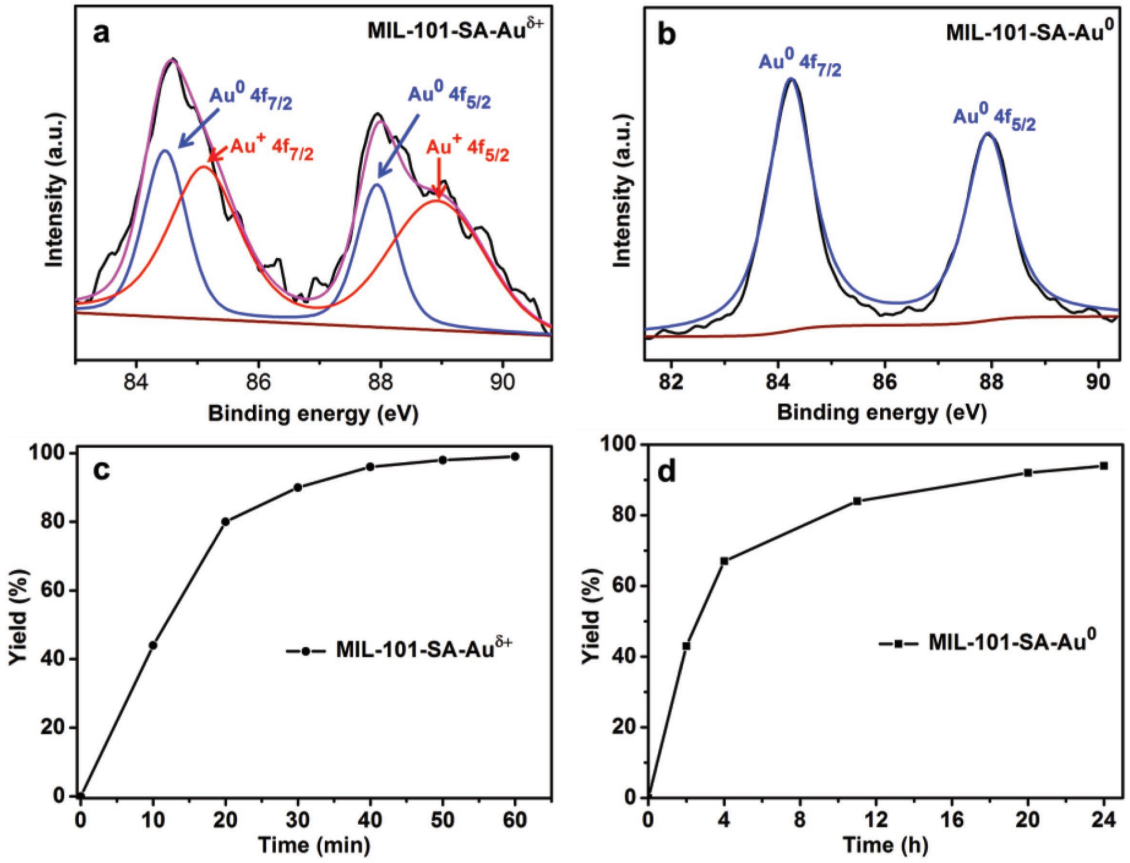

Figure 2. XPS spectra of Au 4f for a) MIL-101-SA-Au$^{\delta+}$ and b) MIL-101-SA-Au^0. The time-dependent yield of the paraformaldehyde, piperidine, and phenylacetylene coupling reaction over c) MIL-101-SA-Au$^{\delta+}$ and d) MIL-101-SA-Au^0.

$$4/3\pi R_{np}^3 = X_{np}\,4/3\pi R_a^3 \quad (2)$$

It can be rearranged to give the following radius relationship between the NP and the atom:

$$R_{np} = X_{np}^{1/3} R_a \quad (3)$$

In the limit of a big NP, the number of surface atoms (X_s) in an NP can be obtained via dividing the surface area of the NP by the cross-sectional area of an atom:

$$X_s = S_{np}/S_a = 4\pi R_{np}^2/(\pi R_a^2) = 4X_{np}^{2/3} \quad (4)$$

Therefore,

$$X_s/X_{np} = 4X_{np}^{2/3}/X_{np} = 4/X_{np}^{1/3} = 4R_a/R_{np} \quad (5)$$

Considering the Au atomic radius (0.144 nm) and the average size of the Au^0 NPs (≈2.7 nm) obtained from the TEM observation for MIL-101-SA-Au^0, ≈43% Au atoms are exposed on the surface. The TOF of MIL-101-SA-Au^0 is calculated to be 36 h^{-1}, while TOF of MIL-101-SA-Au$^{\delta+}$ is as high as 394 h^{-1}. The activity of Au$^{\delta+}$ is approximately 11-fold higher than that of Au^0, clearly suggesting that Au$^{\delta+}$ is the more efficient active species toward the A^3 coupling reaction. In addition, the catalyst poisoning test in the presence of a 1000-fold excess of mercury shows a negligible poisoning effect on the activity of MIL-101-SA-Au$^{\delta+}$, but the catalytic activity of MIL-101-SA-Au^0 is significantly reduced (Figure S6, Supporting Information). This result further confirms that the catalytic activity of MIL-101-SA-Au$^{\delta+}$ does not rely on the possible Au^0 species, even it is present (unobservable in TEM image, Figure 1c). The framework integrity of MIL-101-SA-Au$^{\delta+}$ can be almost maintained, though the activity slightly decreases, during the three consecutive runs (Figure S7, Supporting Information). The TEM observation and XPS spectrum of MIL-101-SA-Au$^{\delta+}$ after three recycling experiment show that a part of Au$^{\delta+}$ species is reduced by the substrate (amine) in the reaction process (Figure S8, Supporting Information). The ICP-AES result shows that ≈8.9% Au species are leached to the reaction solution after three consecutive runs. The slightly decreased activity of MIL-101-SA-Au$^{\delta+}$ in the recycling experiments might be due to the partial reduction of some Au$^{\delta+}$ to Au^0 species and/or the leaching of Au species. In contrast, the activity of MIL-101-SA-Au^0 has no significant change during the three runs (Figure S9a, Supporting Information), and only 0.7% Au species can be detected by ICP-AES in the reaction solution. The XPS spectrum of MIL-101-SA-Au^0 after three recycling experiment shows that all Au species are present in the reduced form (Au^0), and no oxidation state (Au$^{\delta+}$) can be detected (Figure S9b, Supporting Information).

Table 1. Catalytic data for the A^3 coupling of aldehyde, amine, and alkyne over MIL-101-SA-$Au^{\delta+}$ in water.

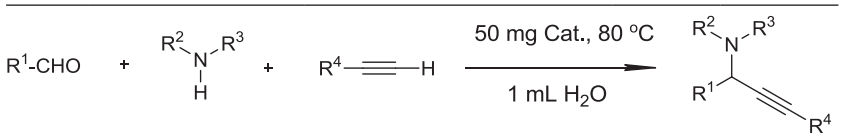

Entry[a)]	R^1-CHO	R^2R^3NH	R^4	T (h)	Yield (%)[b)]
1	$(HCHO)_n$ (R^1 = H)	Piperidine	Ph	1	>99
2	$(HCHO)_n$ (R^1 = H)	Piperidine	2-FC_6H_4	2	>99
3	$(HCHO)_n$ (R^1 = H)	Piperidine	4-$MeOC_6H_4$	2	>99
4	$(HCHO)_n$ (R^1 = H)	Piperidine	n-hexyl	3	98
5	$(HCHO)_n$ (R^1 = H)	Diethylamine	Ph	3	>99
6	$(HCHO)_n$ (R^1 = H)	Diethylamine	2-FC_6H_4	3	>99
7	$(HCHO)_n$ (R^1 = H)	Diethylamine	4-$MeOC_6H_4$	3	>99
8	*n*-Amyl	Piperidine	Ph	20	90

[a)]Reaction conditions: 0.1 mmol alkyne, 0.2 mmol aldehyde, 0.2 mmol amine, 1 mL H_2O, 50 mg MIL-101-SA-$Au^{\delta+}$, 80 °C; [b)]Catalytic reaction product is analyzed and identified by GC.

Encouraged by the excellent catalytic performance of MIL-101-SA-$Au^{\delta+}$, various aldehydes, dialkylamines, and alkynes have also been investigated (**Table 1**). To our delight, good to excellent conversions can be achieved in almost all reactions, indicating the great substrate tolerance of the catalyst. Overall, when the amine and aldehyde are fixed as paraformaldehyde and piperidine, respectively, the reaction activity of phenylacetylene is higher than that of 2-fluorophenylacetylene, 4-ethynylanisole, and 1-octyne (entries 1–4). We assume that the steric hindrance from the large substituents reduces the reaction activity of the latter three substrates. Although the reactivity is a bit lower after changing piperidine to diethylamine, excellent yields can be also obtained when the reaction time length is extended to 3 h (entries 5–7). As an exception, the catalyst attains a relatively low yield (90%) of the target product even after the reaction time length is extended to 20 h when paraformaldehyde is changed to a hexanal (entry 8). A possible reason for this is the relatively lower water solubility of hexanal, which reduces the contact/interaction probability of the substrate with the catalyst.

To further understand the mechanism of A^3 coupling reaction, an Au fluorescent probe (Au-FP) was used to monitor the $Au^{\delta+}$ species during the reaction. Li et al. has demonstrated that Au ions can cause significant change of the emission spectrum of Au-FP.[39] The Au-FP exhibits an absorption peak at 483 nm and a strong emission peak at 636 nm (Figure S10a,b, Supporting Information), which is consistent with that in the reported literature.[39] Moreover, the gas chromatography mass spectrometry (GC-MS) spectrum further demonstrates the existence of Au-FP molecule (Figure S10c, Supporting Information). The emission wavelength of Au-FP in the reaction solution of MIL-101-SA-$Au^{\delta+}$ gives a new fluorescence emission band at 574 nm and a significantly decreased band at 636 nm, while no obvious change can be observed for the Au-FP in the reaction solution of MIL-101-SA-Au^0 (Figure S11, Supporting Information). This striking contrast results clearly manifest that $Au^{\delta+}$ species exists in the reaction system with MIL-101-SA-$Au^{\delta+}$, and the oxidation process of Au^0 to $Au^{\delta+}$ does not take place for MIL-101-SA-Au^0 during the reaction. We propose that the reaction mechanism of MIL-101-SA-$Au^{\delta+}$ might be similar to that with cationic gold under homogeneous conditions (Scheme S2, Supporting Information).[15,40–42] The C—H bond of the alkyne is activated by $Au^{\delta+}$ to give a gold acetylide intermediate (I) which reacts with immonium ion (II), generated from the condensation of aldehyde and amine, to afford the corresponding propargylamine (III) and regenerate the catalytic site.

In summary, the identification of the efficient active site, $Au^{\delta+}$ or Au^0 in the A^3 coupling reaction involving aldehyde, amine and alkyne, remains a debating issue. We have rationally fabricated an ideal model based on MOF platform to meet this challenge. Thanks to the structural tailorability and functionability of the MIL-101-NH_2, the $Au^{\delta+}$ in oxidation state can be well bound to the MOF via the PSM approach. The subsequent treatment in hydrogen/argon flow reduces $Au^{\delta+}$ to Au^0 but does not disturb the MOF structure, which provides an ideal model to identify the more efficient active sites in particular reactions. Unprecedentedly, the TOF of MIL-101-SA-$Au^{\delta+}$ is 11 times higher than that of MIL-101-SA-Au^0 toward the A^3 coupling reaction. This result unambiguously demonstrates that $Au^{\delta+}$ rather than Au^0 behaves as the more efficient active site. This attempt suggests MOFs might be an ideal platform to identify the efficient active centers in the catalytic reactions, indicating the critical role of MOF-based materials in the structure-activity relationship in catalysis.

Supporting Information

Supporting Information is available from the Wiley Online Library or from the author.

Acknowledgements

This work was supported by the NSFC (21725101, 21673213, and 21521001), the National Research Fund for Fundamental Key Project (2014CB931803), and the Fundamental Research Funds for the Central Universities (WK2060030029).

Conflict of Interest

The authors declare no conflict of interest.

Keywords

A^3 coupling, active site identification, Au catalysis, metal–organic frameworks

Received: June 29, 2018
Revised: August 30, 2018
Published online: October 4, 2018

[1] H.-L. Jiang, B. Liu, T. Akita, M. Haruta, H. Sakurai, Q. Xu, *J. Am. Chem. Soc.* **2009**, *131*, 11302.
[2] M. Shekhar, J. Wang, W.-S. Lee, W. D. Williams, S. M. Kim, E. A. Stach, J. T. Miller, W. N. Delgass, F. H. Ribeiro, *J. Am. Chem. Soc.* **2012**, *134*, 4700.
[3] Y. Zhu, H. Qian, B. A. Drake, R. Jin, *Angew. Chem., Int. Ed.* **2010**, *49*, 1295.
[4] M. Turner, V. B. Golovko, O. P. H. Vaughan, P. Abdulkin, A. Berenguer-Murcia, M. S. Tikhov, B. F. G. Johnson, R. M. Lambert, *Nature* **2008**, *454*, 981.
[5] R. Cai, X. Ye, Q. Sun, Q. He, Y. He, S. Ma, X. Shi, *ACS Catal.* **2017**, *7*, 1087.
[6] A. S. K. Hashmi, G. J. Hutchings, *Angew. Chem., Int. Ed.* **2006**, *45*, 7896.
[7] T. Ishida, M. Haruta, *Angew. Chem., Int. Ed.* **2007**, *46*, 7154.
[8] X. Zhang, F. X. LlabrésI. Xamena, A. Corma, *J. Catal.* **2009**, *265*, 155.
[9] B. T. Elie, C. Levine, I. Ubarretxena-Belandia, A. Varela-Ramírez, R. J. Aguilera, R. Ovalle, M. Contel, *Eur. J. Inorg. Chem.* **2009**, *2009*, 3421.
[10] K. K. R. Datta, B. V. S. Reddy, K. Ariga, A. Vinu, *Angew. Chem., Int. Ed.* **2010**, *49*, 5961.
[11] Y. Jiang, X. Zhang, X. Dai, W. Zhang, Q. Sheng, H. Zhuo, Y. Xiao, H. Wang, *Nano Res.* **2017**, *10*, 876.
[12] X. Zhang, A. Corma, *Angew. Chem., Int. Ed.* **2008**, *47*, 4358.
[13] L. Liu, X. Tai, N. Zhang, Q. Meng, C. Xin, *React. Kinet., Mech. Catal.* **2016**, *119*, 335.
[14] L. Liu, X. Tai, X. Zhou, C. Xin, Y. Yan, *Sci. Rep.* **2017**, *7*, 12709.
[15] C. Wei, C.-J. Li, *J. Am. Chem. Soc.* **2003**, *125*, 9584.
[16] F.-X. Zhu, W. Wang, H.-X. Li, *J. Am. Chem. Soc.* **2011**, *133*, 11632.
[17] H.-C. Zhou, J. R. Long, O. M. Yaghi, *Chem. Rev.* **2012**, *112*, 673.
[18] A. Dhakshinamoorthy, A. M. Asiri, H. García, *Angew. Chem., Int. Ed.* **2016**, *55*, 5414.
[19] Q.-L. Zhu, Q. Xu, *Chem. Soc. Rev.* **2014**, *43*, 5468.
[20] B. Li, H.-M. Wen, Y. Cui, W. Zhou, G. Qian, B. Chen, *Adv. Mater.* **2016**, *28*, 8819.
[21] Q.-G. Zhai, X. Bu, C. Mao, X. Zhao, P. Feng, *J. Am. Chem. Soc.* **2016**, *138*, 2524.
[22] L. E. Kreno, K. Leong, O. K. Farha, M. Allendorf, R. P. V. Duyne, J. T. Hupp, *Chem. Rev.* **2012**, *112*, 1105.
[23] H. R. Moon, D.-W. Lim, M. P. Suh, *Chem. Soc. Rev.* **2013**, *42*, 1807.
[24] Y.-B. Huang, J. Liang, X.-S. Wang, R. Cao, *Chem. Soc. Rev.* **2017**, *46*, 126.
[25] Q. Yang, Q. Xu, H.-L. Jiang, *Chem. Soc. Rev.* **2017**, *46*, 4774.
[26] P. Horcajada, F. Salles, S. Wuttke, T. Devic, D. Heurtaux, G. Maurin, A. Vimont, M. Daturi, O. David, E. Magnier, N. Stock, Y. Filinchuk, D. Popov, C. Riekel, G. Férey, C. Serre, *J. Am. Chem. Soc.* **2011**, *133*, 17839.
[27] S. M. Cohen, *J. Am. Chem. Soc.* **2017**, *139*, 2855.
[28] B. An, L. Zeng, M. Jia, Z. Li, Z. Lin, Y. Song, Y. Zhou, J. Cheng, C. Wang, W. Lin, *J. Am. Chem. Soc.* **2017**, *139*, 17747.
[29] G. Férey, C. Mellot-Draznieks, C. Serre, F. Millange, J. Dutour, S. Surblé, I. Margiolaki, *Science* **2005**, *309*, 2040.
[30] S. Bernt, V. Guillerm, C. Serre, N. Stock, *Chem. Commun.* **2011**, *47*, 2838.
[31] J. Tang, W. Dong, G. Wang, Y. Yao, L. Cai, Y. Liu, X. Zhao, J. Xua, L. Tan, *RSC Adv.* **2014**, *4*, 42977.
[32] Z.-Q. Bai, L.-Y. Yuan, L. Zhu, Z.-R. Liu, S.-Q. Chu, L.-R. Zheng, J. Zhang, Z.-F. Chai, W.-Q. Shi, *J. Mater. Chem. A* **2015**, *3*, 525.
[33] Y. Li, J. Tang, L. He, Y. Liu, Y. Liu, C. Chen, Z. Tang, *Adv. Mater.* **2015**, *27*, 4075.
[34] X. Zhang, H. Shi, B.-Q. Xu, *Catal. Today* **2007**, *122*, 330.
[35] K. Qian, W. Huang, J. Fang, S. Lv, B. He, Z. Jiang, S. Wei, *J. Catal.* **2008**, *255*, 269.
[36] K. Leus, P. Concepcion, M. Vandichel, M. Meledina, A. Grirrane, D. Esquivel, S. Turner, D. Poelman, M. Waroquier, V. Van Speybroeck, G. Van Tendeloo, H. H. García, P. Van Der Voort, *RSC Adv.* **2015**, *5*, 22334.
[37] J. H. Carter, S. Althahban, E. Nowicka, S. J. Freakley, D. J. Morgan, P. M. Shah, S. Golunski, C. J. Kiely, G. J. Hutchings, *ACS Catal.* **2016**, *6*, 6623.
[38] R. L. Johnston, *Atomic and Molecular Clusters*, Taylor & Francis, New Fetter Lane, London **2002**.
[39] Z. Li, Y. Xu, J. Fu, H. Zhu, Y. Qian, *Chem. Commun.* **2018**, *54*, 888.
[40] V. K.-Y. Lo, K. K.-Y. Kung, M.-K. Wong, C.-M. Che, *J. Organomet. Chem.* **2009**, *694*, 583.
[41] M. J. Campbell, F. D. Toste, *Chem. Sci.* **2011**, *2*, 1369.
[42] Q. Zhang, M. Cheng, X. Hu, B.-G. Li, J.-X. Ji, *J. Am. Chem. Soc.* **2010**, *132*, 7256.